Extended Data Fig. 1: Signaling competency and preparation of NTS-NTSR1-Gi complex in cNDs.

From: Cryo-EM structure of an activated GPCR–G protein complex in lipid nanodiscs

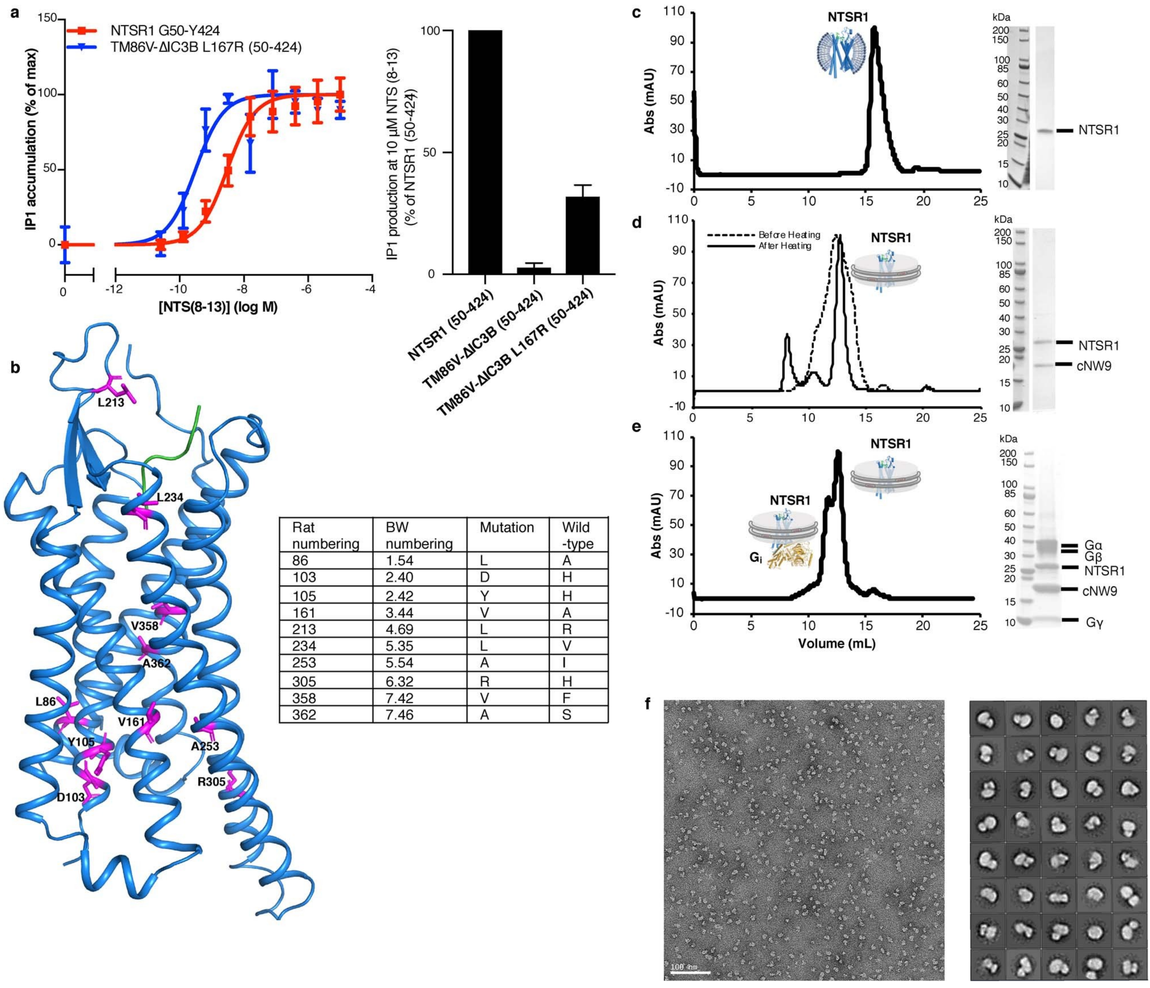

Rat numbering	BW numbering	Mutation	Wild -type
86	1.54	L	A
103	2.40	D	H
105	2.42	Y	H
161	3.44	V	A
213	4.69	L	R
234	5.35	L	V
253	5.54	A	I
305	6.32	R	H
358	7.42	V	F
362	7.46	A	S

a, Signaling competency of NTSR1 constructs. Wild-type NTSR1 (50-424) or NTSR1 variants were transiently transfected into HEK293T/17 cells, and activation of $G\alpha_q$ signaling was quantified by measuring inositol-1-phosphate (IP1) accumulation after stimulation with NTS_{8-13}. Data were normalized to receptor expression at the cell surface and are shown as mean and s.e.m. of n = 4 independent experiments (each performed in duplicate). Left, dose dependent IP1 production expressed as percentage of IP1 accumulation at maximal ligand concentration. Fitting of the curves result in EC50 of 2.7 nM for wild-type NTSR1 and 0.22 nM for TM86V ΔIC3B L167R. Right, bar graph showing IP1 production level at 10 μM agonist NTS_{8-13}. The NTSR1 variant TM86V ΔIC3B lacking the L167R back mutation exhibits no IP1 production, suggesting a critical role of $R167^{3.50}$ in signal transduction. **b**, Residues mutated in the TM86V-L167R construct shown as magenta sticks on the left and listed in the table on the right. **c-e**, Size-exclusion chromatograms and corresponding SDS-PAGE gels for (**c**) NTSR1 in DH_7PC detergent micelles, (**d**) NTSR1 in POPC/POPG cNW9 nanodiscs before (dashed line) and after (solid line) heating, and (**e**) NTSR1-G_i complex in POPC/POPG cNW9 nanodiscs. **f**, Fractions corresponding to the NTS-NTSR1-G_i complex in (**e**) were analyzed by negative-stain EM, and then used for cryo-EM structure determination. Left, representative negative-stain EM micrograph of NTS-NTSR1-G_i complexes in cNDs. Right, 2D class averages.

Back to article page ›

Nature Structural & Molecular Biology | ISSN 1545-9985 (online)

Extended Data Fig. 2: Characterization of the binding kinetics between NTS-NTSR1 and G_i in cNDs.

From: Cryo-EM structure of an activated GPCR–G protein complex in lipid nanodiscs

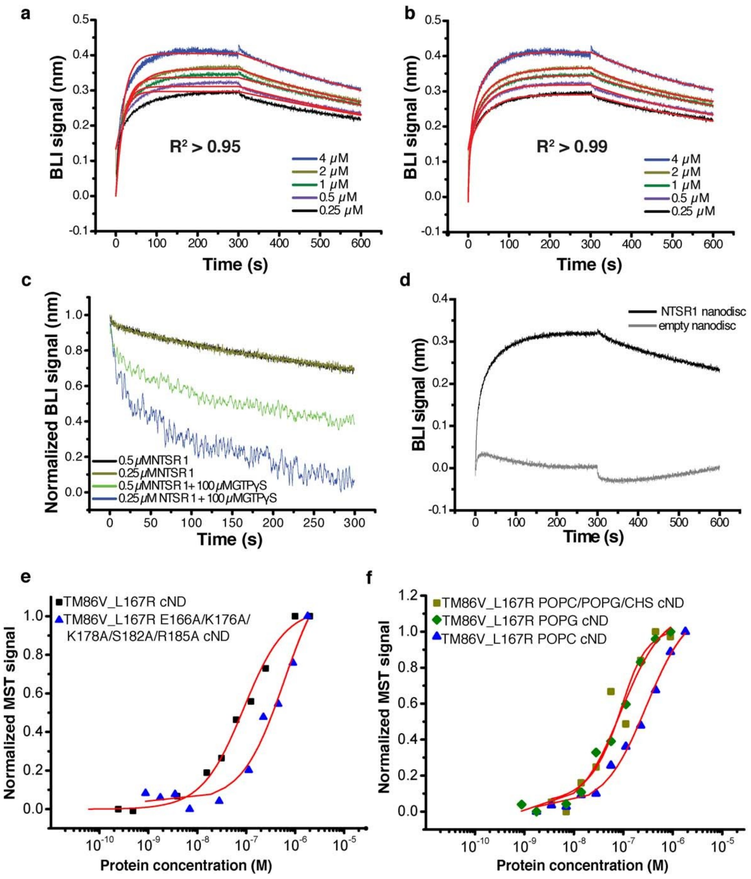

	k_{on} (1/M*s)	k_{off} (1/s)	K_D(nM)
Mode 1	$2.9\pm0.1\times10^{5}$	$1.7\pm0.2\times10^{-3}$	5.8±1.6
Mode 2	$6.4\pm0.3\times10^{4}$	$2.5\pm0.2\times10^{-3}$	38±11

	K_D (nM)
TM86V-L167R POPC/POPG (3/2) cND	76 ± 18
TM86V-L167R E166A/K176A/K178A/S182A/R185A POPC/POPG (3/2) cND	347 ± 129
TM86V-L167R POPC cND	236 ± 52
TM86V-L167R POPG cND	53 ± 39
TM86V-L167R POPC/POPG/CHS (3/2/0.3) cND	46 ± 20

a-b, Fitting of Bio-Layer Interferometry (BLI) traces of G_i binding to NTS-NTSR1-cND using (**a**) one binding mode and (**b**) two binding mode shows better fitting using two binding mode. Right, a table showing k_{on}, k_{off} and K_D from the two binding mode fitting. **c**, Dissociation between G_i and NTS-NTSR1-cND in the absence (black and brown) and presence (green and blue) of GTPγS, showing faster dissociation of the complex in the presence of GTPγS, suggesting that the NTSR1-$G\alpha_{i1}\beta_1\gamma_1$ complex in cNDs is capable of GDP/GTP exchange. **d**, Association and dissociation kinetics of G_i binding to NTS-NTSR1-cND (dark) and empty cND (gray), showing much slower association and faster dissociation of G_i binding to empty cND compared to NTS-NTSR1-cND, suggesting that interaction between G_i and NTS-NTSR1-cND is driven by G_i binding to NTSR1 rather than to the nanodisc. **e**, Microscale thermophoresis (MST) data for the binding between NTSR1 and G_i (square mark), as well as the binding between mutant TM86V-L167R E166A/K176A/K178A/S182A/R185A and G_i (triangle mark) in POPC/POPG (3/2) cND. **f**, MST data for the binding between NTSR1 and G_i in POPC cND (triangle mark), POPG cND (diamond mark) and POPC/POPG/CHS cND (square mark). Right, a table showing K_D from **e-f**.

Back to article page >

Nature Structural & Molecular Biology | ISSN 1545-9985 (online)

Extended Data Fig. 3: Cryo-EM data processing.

From: Cryo-EM structure of an activated GPCR–G protein complex in lipid nanodiscs

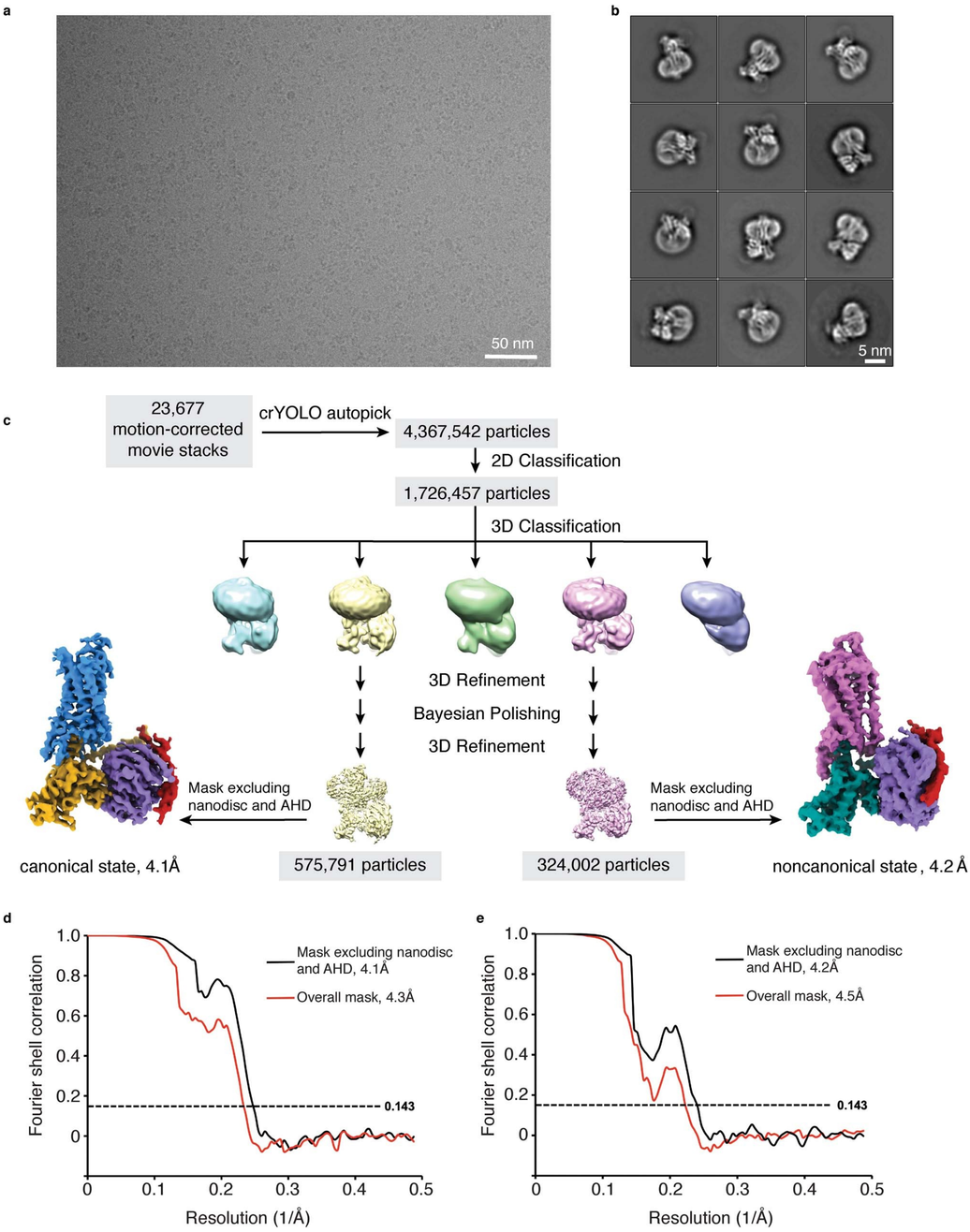

a, Representative micrograph showing the distribution of NTS-NTSR1-G_i-cND particles in vitreous ice. **b**, Selected two-dimensional class averages showing secondary structure features. The cND has an approximate diameter of 9 nm. **c**, Simplified flow chart of the cryo-EM processing. Two datasets were collected and processed similarly; the number of particles shown here are a conflation of both datasets. Two well-resolved classes corresponding to canonical and noncanonical states were identified. Further rounds of classification did not identify additional classes or improve the resolution or map quality. **d,e**, Fourier shell correlation (FSC) curves for the (**d**) canonical state and (**e**) noncanonical state with masks that either include or exclude the cND and AHD.

Back to article page ›

Nature Structural & Molecular Biology | ISSN 1545-9985 (online)

Extended Data Fig. 4: Cryo-EM density.

From: Cryo-EM structure of an activated GPCR–G protein complex in lipid nanodiscs

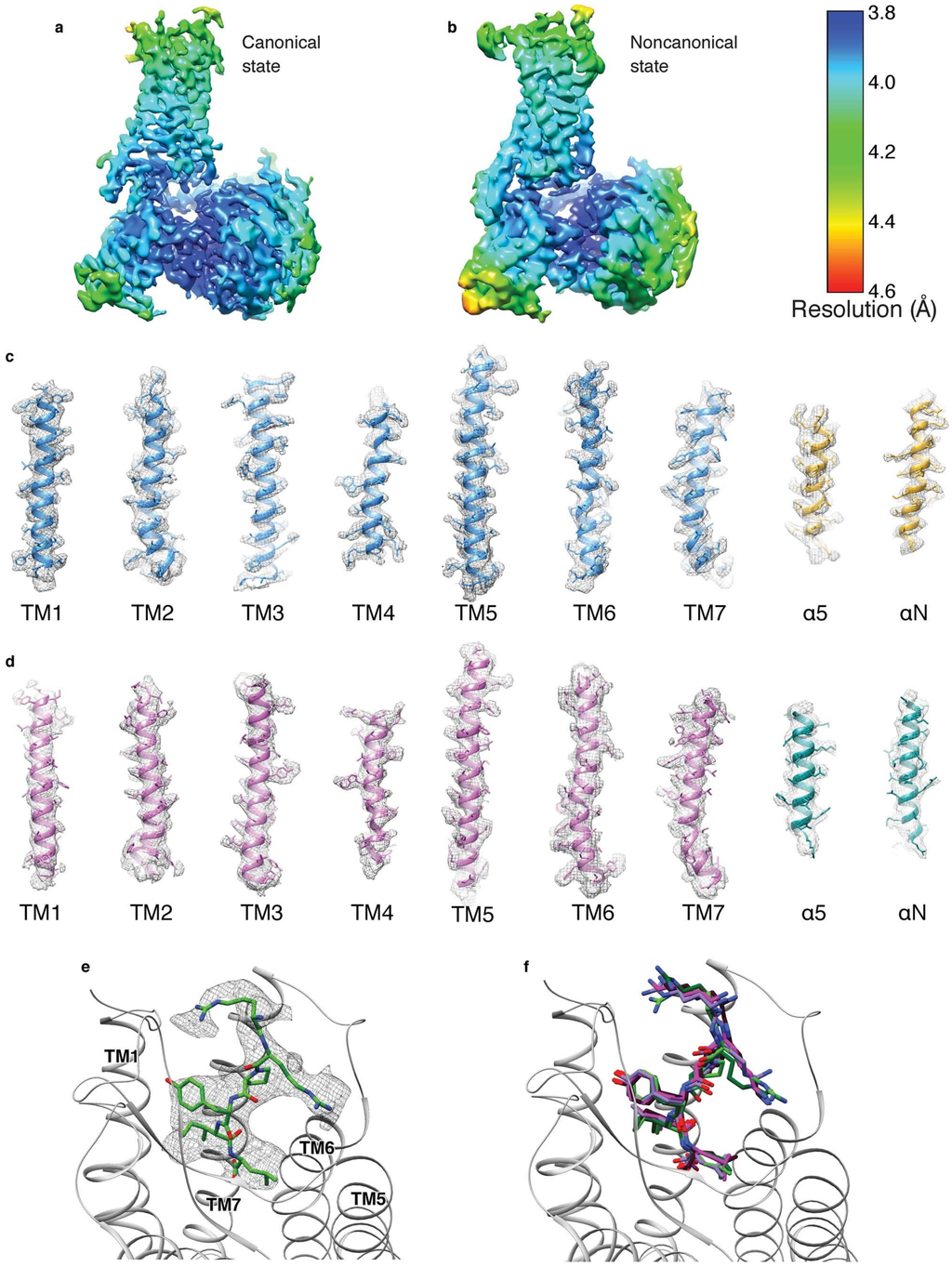

a,b, Local resolution of the NTS-NTSR1-G_i complex in the (**a**) canonical state and (**b**) noncanonical state. The local resolution was calculated in RELION-3. **c,d**, Density and model for the transmembrane helices of NTSR1 and the α5 and αN-helices of $G\alpha_{i1}$ in the (**c**) canonical state and (**d**) noncanonical state. **e**, Density and model for NTS_{8-13}. **f**, Superposition of the atomic models of NTS_{8-13} from the NTS-NTSR1-G_i-cND complex in the canonical (light green), and noncanonical state (dark green) with NTS from the NTS-NTSR1 crystal structure (purple; PDB 4XEE) and JMV449 (an NTS analog) from the NTSR1-G_i-detergent complex in the canonical (magenta; PDB 6OS9) and noncanonical state (dark red; PDB 6OSA).

Back to article page ›

Nature Structural & Molecular Biology | ISSN 1545-9985 (online)

Extended Data Fig. 5: Structure and position of the α-helical domain (AHD).

From: Cryo-EM structure of an activated GPCR–G protein complex in lipid nanodiscs

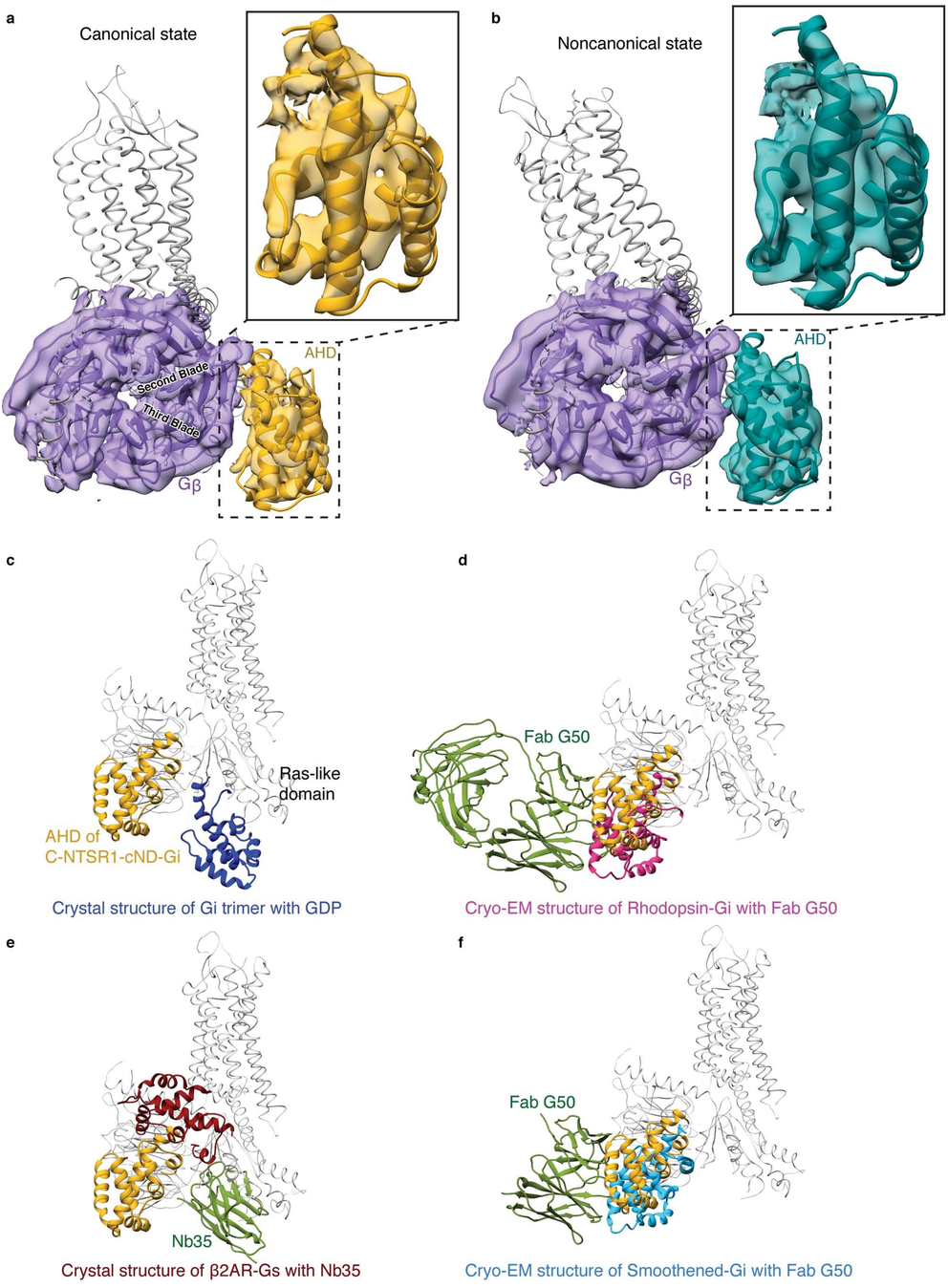

a, Density maps and models showing the interaction between $G\beta_1$ (purple) and $G\alpha_{i1}$ AHD (gold) in the canonical state. Zoom-in view of the $G\alpha_{i1}$ AHD is shown. **b**, Density maps and models showing the interaction between $G\beta_1$ (purple) and $G\alpha_{i1}$ AHD (dark green) in the noncanonical state. Zoom-in view of the $G\alpha_{i1}$ AHD is shown. The models in (**a**) and (**b**) are superposed on the $G\beta_1$ subunits and are shown in the same view. AHD in both states interacts with the second and third blades of $G\beta_1$. **c**-**f**, Comparison of the AHD of the canonical state NTS-NTSR1-Gi-cND (gold) with **c**, A crystal structure of GDP-G_i (blue; PDB 1GP2), **d**, A crystal structure of β_2AR-G_s with nanobody Nb35 (AHD is dark red and Nb35 is green; PDB 3SN6), **e**, A cryo-EM structure of Rhodopsin–G_i with Fab G50 (AHD is pink and Fab G50 is green; PDB 6CMO), and **f**, A cryo-EM structure of Smoothened-G_i with Fab G50 (AHD is light blue and Fab G50 is green; PDB 6OT0). The models are superposed on the Gα Ras-like domain.

Back to article page ›

Nature Structural & Molecular Biology | ISSN 1545-9985 (online)

Extended Data Fig. 6: Cryo-EM structure of the NTS-NTSR1-G_i complex in lipid nanodiscs and the interaction with lipid.

From: Cryo-EM structure of an activated GPCR–G protein complex in lipid nanodiscs

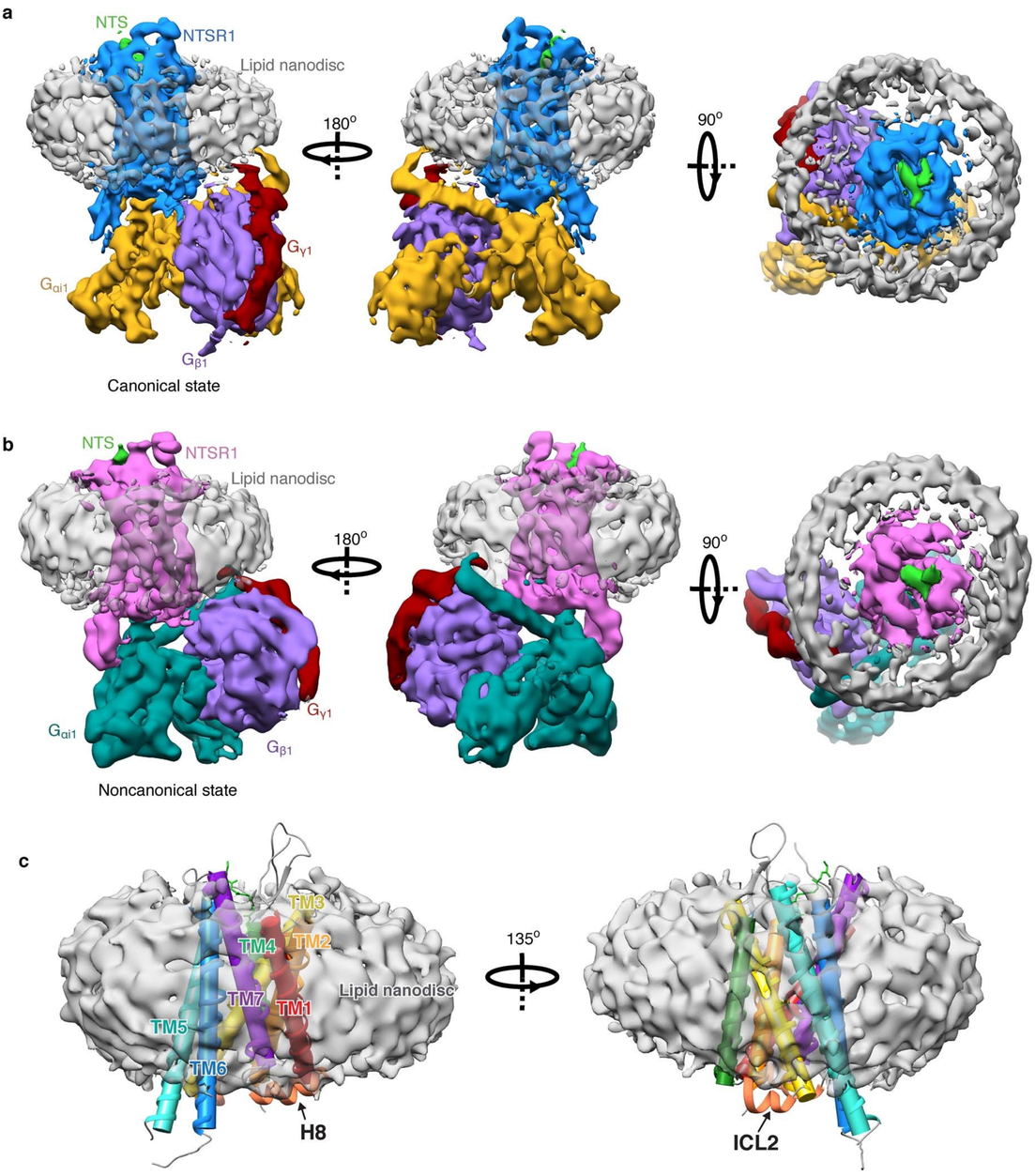

a, Three views of the cryo-EM density map of the NTS-NTSR1-G_i-cND complex in the canonical state. **b**, Three views of the cryo-EM density map of the NTS-NTSR1-G_i-cND complex in the noncanonical state. The maps in panels (a) and (b) are low-pass filtered to 5 Å and colored by subunit. **c**, Two views of NTS-NTSR1 surrounded by nanodisc density. The transmembrane helices are shown in cylinder representation using the rainbow coloring scheme. ICL2 and helix H8 are partially submerged in lipid.

Back to article page >

Nature Structural & Molecular Biology | ISSN 1545-9985 (online)

Extended Data Fig. 7: Impact of the lipid bilayer on the structure of NTSR1.

From: Cryo-EM structure of an activated GPCR–G protein complex in lipid nanodiscs

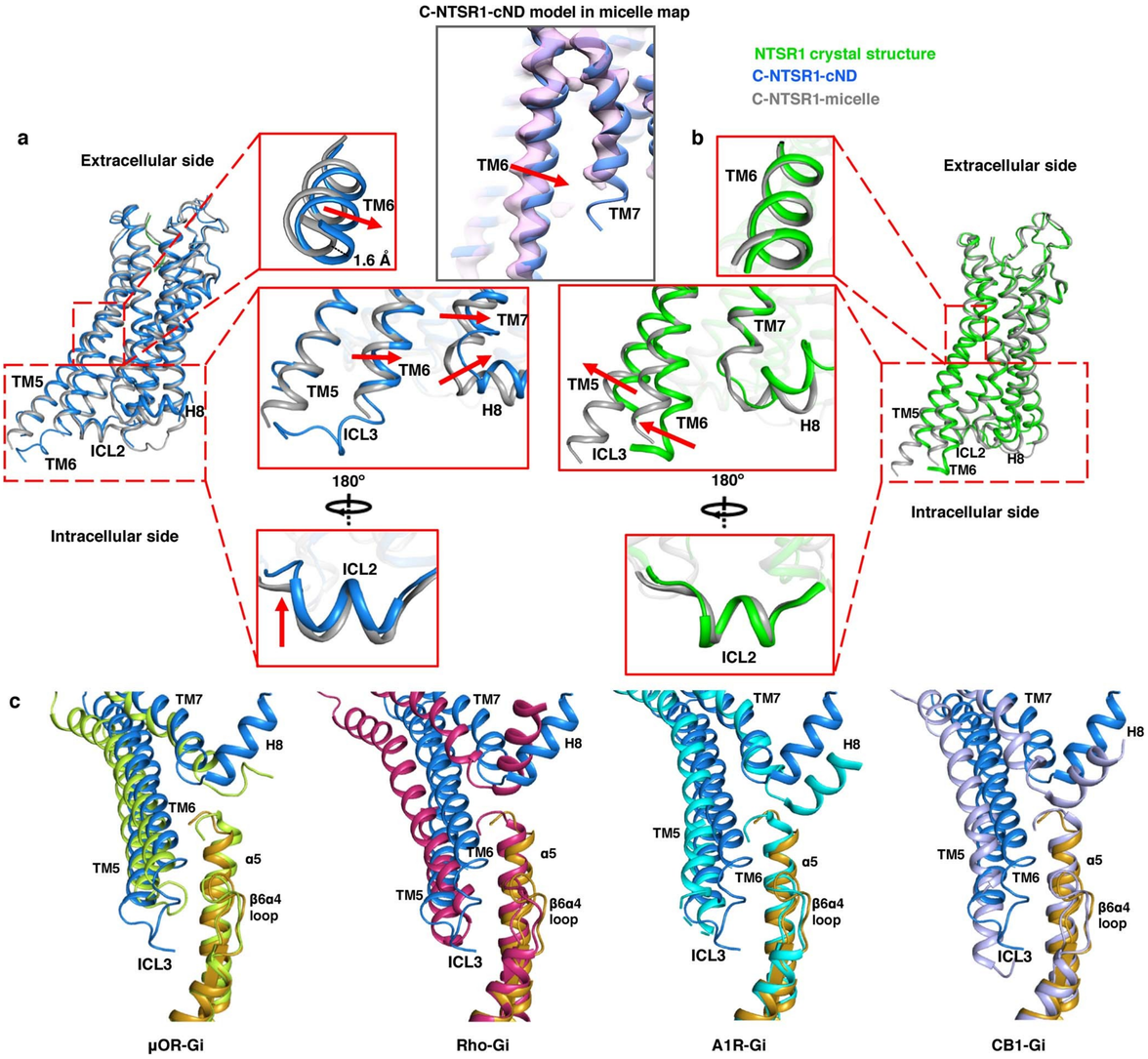

a, Comparison between the cryo-EM structures of the canonical states of NTSR1 (with G_i) in lipid bilayer (blue) and detergent (gray, PDB 6OS9). TM6 is shifted by 1.6 Å (based on Cα of V309) inwards in lipid bilayer. Right, comparison of the C-NTS-NTSR1-Gi-cND model (blue) with the density map of C-NTSR1-Gi-micelle (pink) (EMD-20180, low-pass filtered to 5 Å) confirms this shift to be significant. **b**, Structural comparison between the crystal structure of NTSR1 in detergent (green, PDB 4XEE) and the cryo-EM structure of the canonical state of NTSR1 in complex with G_i in detergent (gray, PDB 6OS9). The atomic models in (a) and (b) are superposed on NTSR1. **c**, Comparison of the localization of TM5-TM6 relative to α5-helix of Gα in class A GPCR-G_i complex structures, including the canonical state NTSR1 (blue) in complex with G_i (gold) structure reported in the current study, μOR-G_i (lime green; PDB 6DDE), Rho-G_i (hot pink; PDB 6CMO), A_1R-G_i (cyan; PDB 6D9H), and CB1-G_i (purple; PDB 6N4B). The models are superposed on the Ras-like domain of Gα.

Back to article page >

Nature Structural & Molecular Biology | ISSN 1545-9985 (online)

Extended Data Fig. 8: ICL2 interaction with a hydrophobic pocket of G_i.

From: Cryo-EM structure of an activated GPCR–G protein complex in lipid nanodiscs

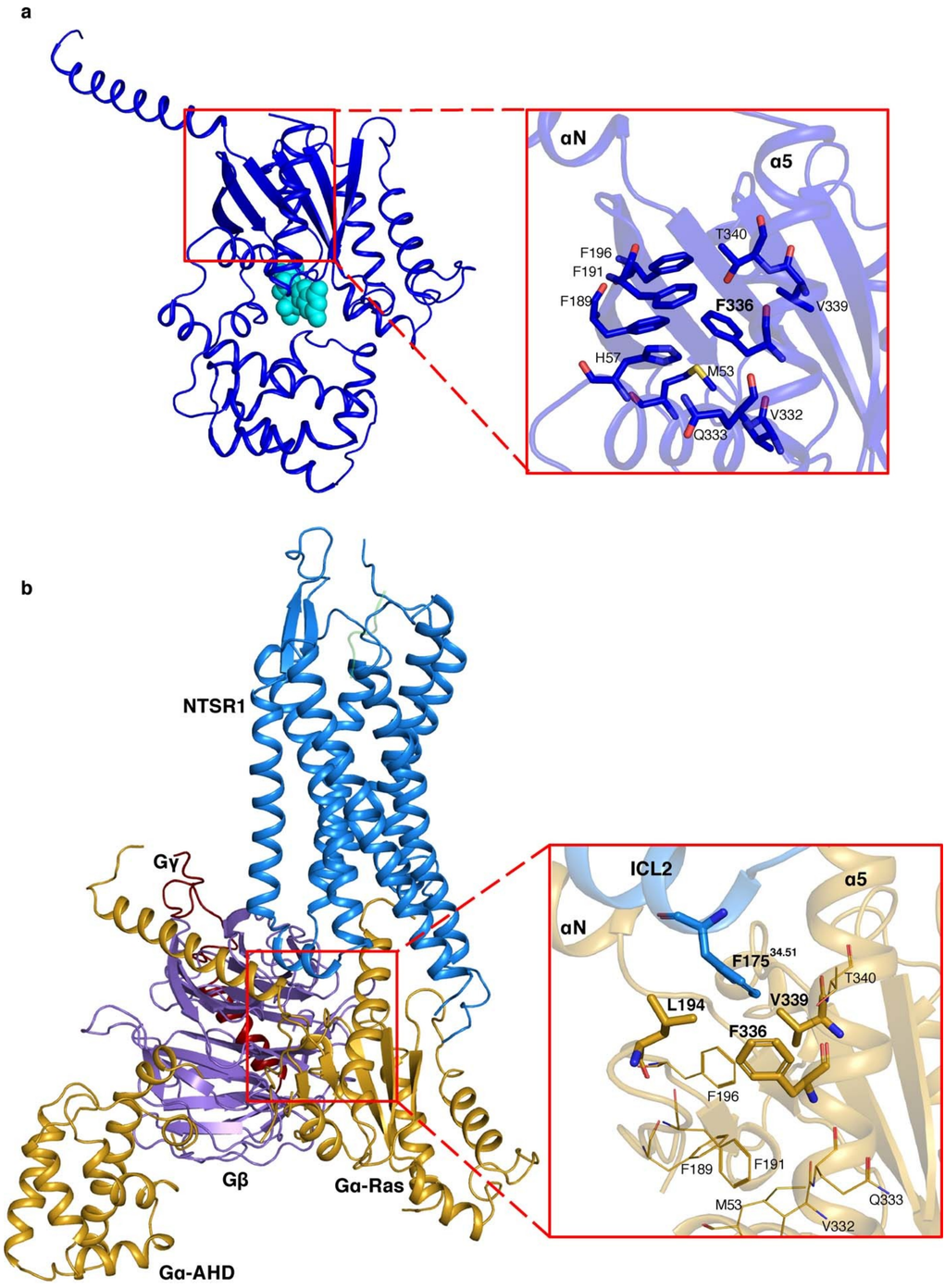

a, Structure of GDP-$G\alpha_i$ showing a hydrophobic network surrounding F336 in the zoomed-in view. Residues involved in the network are shown as sticks. **b**, Atomic model of C-NTS-NTSR1-G_i-cND showing insertion of $F175^{34.51}$ from ICL2 of NTSR1 into a hydrophobic pocket involving residues F336, L194 and V339 of $G\alpha_i$. Residues involved in the network are shown as sticks. Residues from the network in (**a**) are shown in lines. A transition of F336 on $G\alpha_i$ from the network in (**a**) in the GDP-bound state to a new network in (**b**) in the NTSR1-bound state is observed.

Back to article page ›

Nature Structural & Molecular Biology | ISSN 1545-9985 (online)

Extended Data Fig. 9: Comparison of NTSR1-G_i interaction in lipid bilayer with detergent micelles.

From: Cryo-EM structure of an activated GPCR–G protein complex in lipid nanodiscs

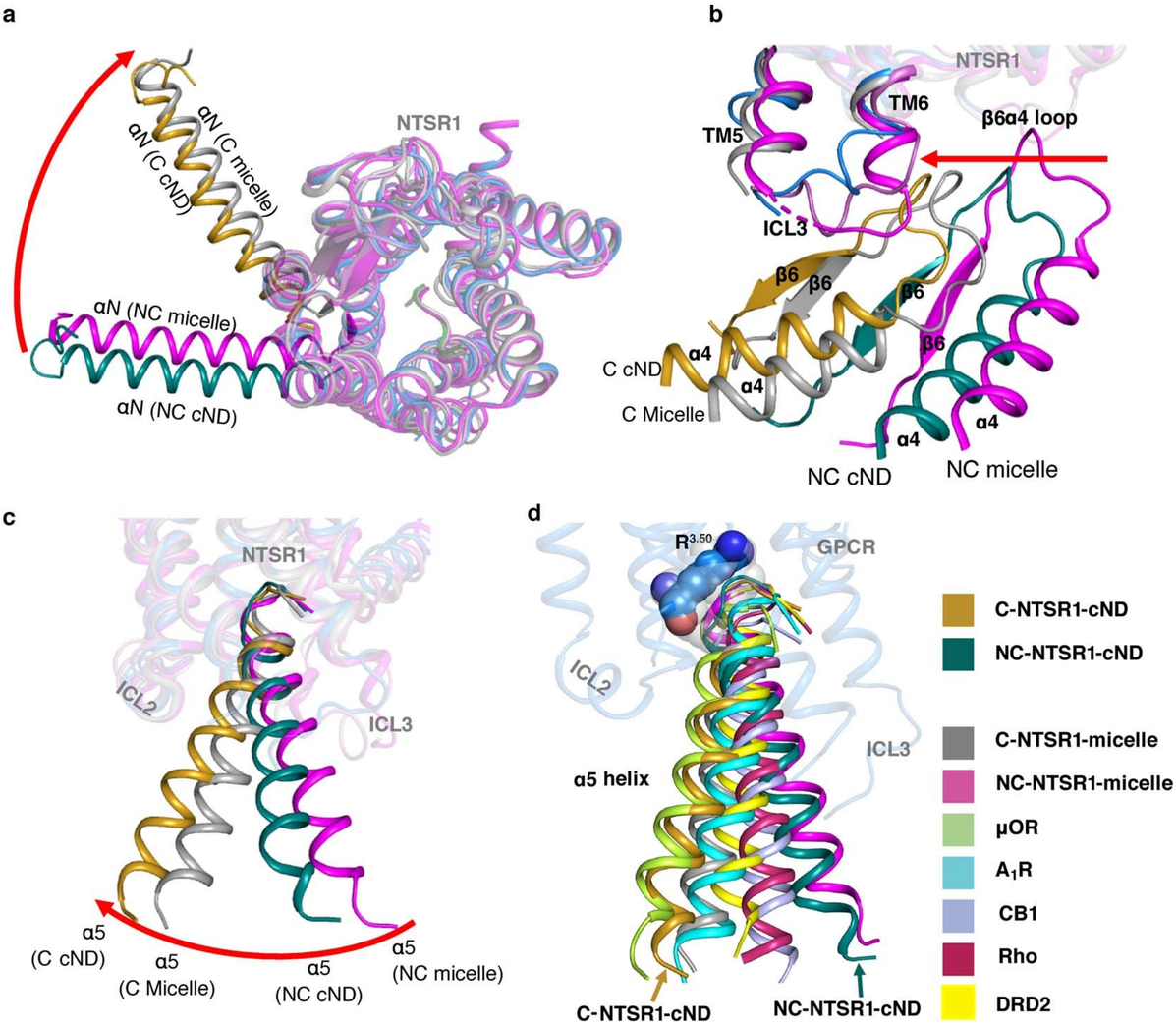

a-c, Superposed structure of C-state NTSR1 (blue) and Gα (gold) in cND, NC-state NTSR1 (orchid) and Gα (dark cyan) in cND, C-state NTSR1 and Gα in micelle (gray, PDB 6OS9), NC-state NTSR1 and Gα in micelle (magenta, 6OSA). The models are superposed on NTSR1. **a**, extracellular view of NTSR1 and αN-helix; **b**, side view of NTSR1 ICL3 and α4β6 loop; **c**, side view of NTSR1 and α5-helix. **d**, Comparison of the localization of α5-helix relative to GPCR in class A GPCR-G_i complex structures, including the canonical (gold) state and noncanonical (dark cyan) state structure reported in the current study, canonical (gray) and noncanonical (magenta) state of NTSR1-G_i in detergent micelle, μOR-G_i (lime green; PDB 6DDE), A_1R-G_i (cyan; PDB 6D9H), CB1-G_i (purple; PDB 6N4B), Rho-G_i (hot pink; PDB 6CMO) and DRD2–G_i (yellow; PDB 6VMS). The structures are superposed on the GPCR. Residue $R^{3.50}$ is shown as colored spheres in C-state NTSR1 and as partially transparent gray spheres in the other GPCRs.

Back to article page >

Nature Structural & Molecular Biology | ISSN 1545-9985 (online)

Extended Data Fig. 10: Molecular dynamics (MD) simulation for the interaction between ICL3 and the α4β6 loop.

From: Cryo-EM structure of an activated GPCR–G protein complex in lipid nanodiscs

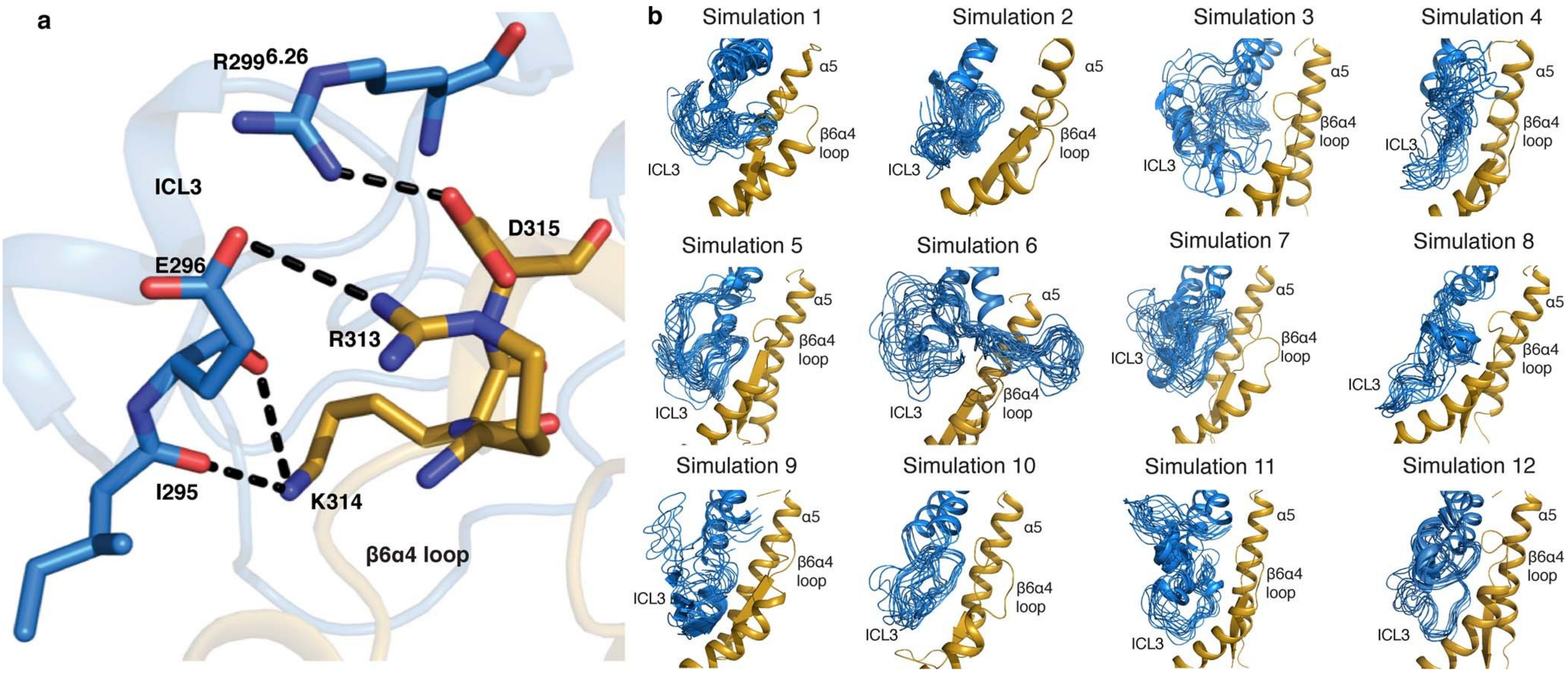

a, MD simulation showing the salt bridges and hydrogen bonds that form between TM6-ICL3 and α4β6 loop in the canonical state of NTS-NTSR1-Gi-cND represented by simulation 12. **b**, Dynamics of ICL3 for each independent simulation of the canonical state of NTS-NTSR1-G_i-cND. Frames are sampled every 40 ns from each individual simulation. All 12 simulations show various interactions including salt bridges/hydrogen bonds between ICL3 and the α4β6 loop. An example of detailed interactions is shown in (**a**). NTSR1 is colored in blue and G_i in gold in (**a,b**).

Back to article page ›

Nature Structural & Molecular Biology | ISSN 1545-9985 (online)

nature portfolio

https://doi.org/10.1038/s41594-020-00554-6

Supplementary information

Cryo-EM structure of an activated GPCR–G protein complex in lipid nanodiscs

In the format provided by the authors and unedited

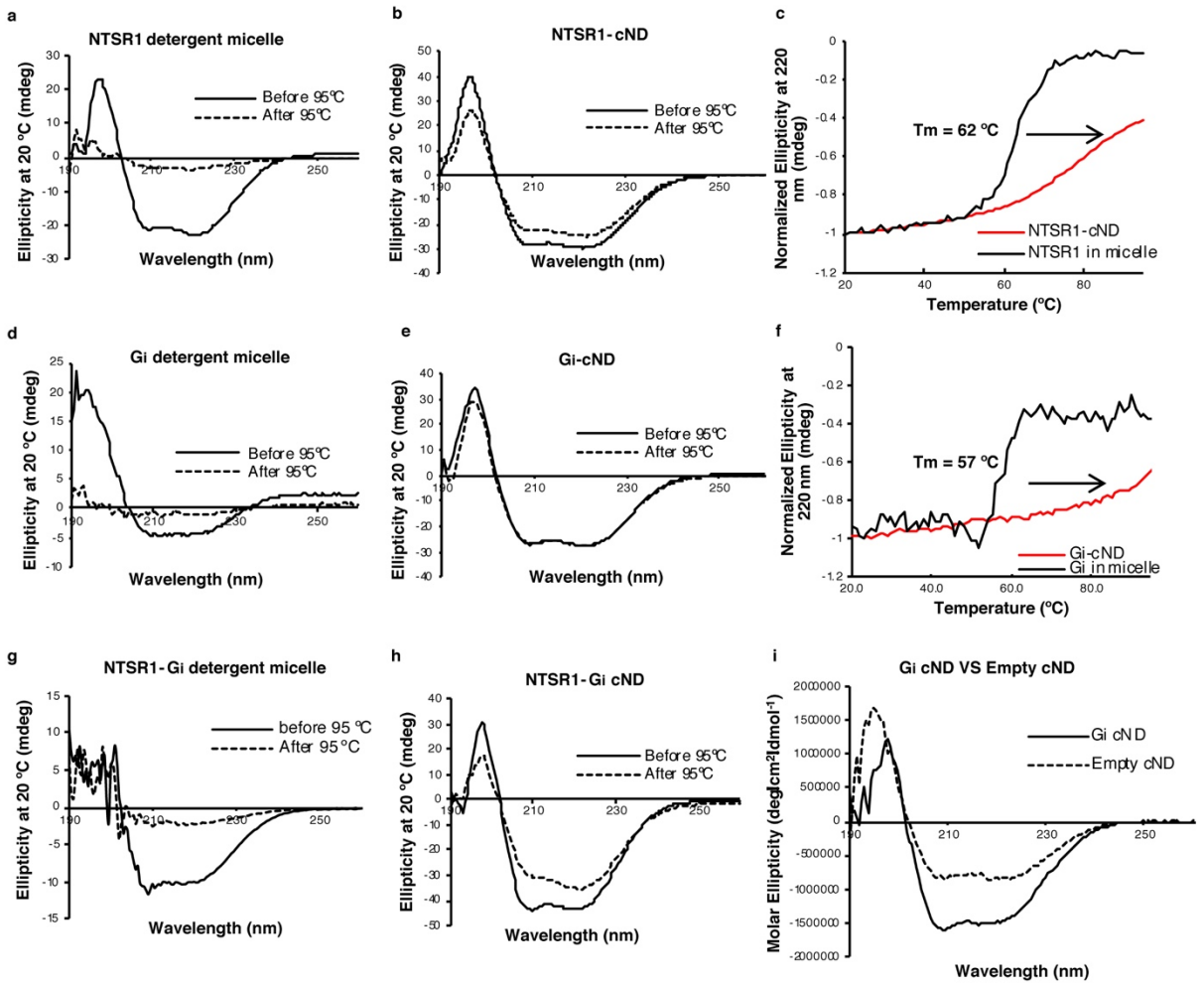

Supplementary Fig. 1 | Thermostability enhancement of NTSR1, G_i, and NTSR1-G_i complexes by incorporation into cNDs. **a-b**, Circular Dichroism (CD) spectra at 20 ºC before (solid line) and after (dashed line) treatment at 95 ºC of (**a**) NTSR1 in DH_7PC detergent micelles; (**b**) NTSR1 in cNDs. **c**, Temperature-dependent CD signals of NTSR1 in detergent micelles (black) and cNDs (red) at 220 nm. **d-e**, CD spectra at 20 ºC before (solid line) and after (dashed line) treatment at 95 ºC of (**d**) G_i in DH_7PC detergent micelles; (**e**) G_i in cNDs. G_i was reconstituted into cNDs by incubation with POPC/POPG lipid, cNW9, and cholate, followed by detergent removal and size-exclusion chromatography. **f**, Temperature-dependent CD signals of G_i in detergent micelles (black) and cNDs (red) at 220 nm. The melting temperature (Tm) of cNDs is 93 ºC (data

not shown) and therefore does not affect transitions before this temperature. **g-h**, CD spectra at 20 ºC before (solid line) and after (dashed line) treatment at 95 ºC of (**g**) NTSR1-G_i in LMNG/GDN/CHS detergent micelles; (**h**) NTSR1-G_i in cNDs. **i**, CD spectra of 2 μM G_i-cND (solid line) and 2 μM empty cND (dashed line), showing nearly 50% signal contribution from G_i. NTSR1 and G_i account for at least 50% of CD signals even in the presence of cNDs. NTSR1 in detergent micelles irreversibly unfolds during temperature increase with a Tm of 62 ºC. In contrast, NTSR1-cND changes structure around 80 ºC and does not lose much secondary structure after decreasing temperature to 20 ºC. Similar observations were made for G_i, where the protein irreversibly and completely unfolds with Tm of 57 ºC in detergent micelles but displays no clear transition temperature in cNDs. For the NTSR1-G_i complex in cND, only mild unfolding was observed around 82 ºC. These observations indicate that lipid bilayers improve the stability of NTSR1, G_i and NTSR1-G_i complexes relative to detergent micelles.

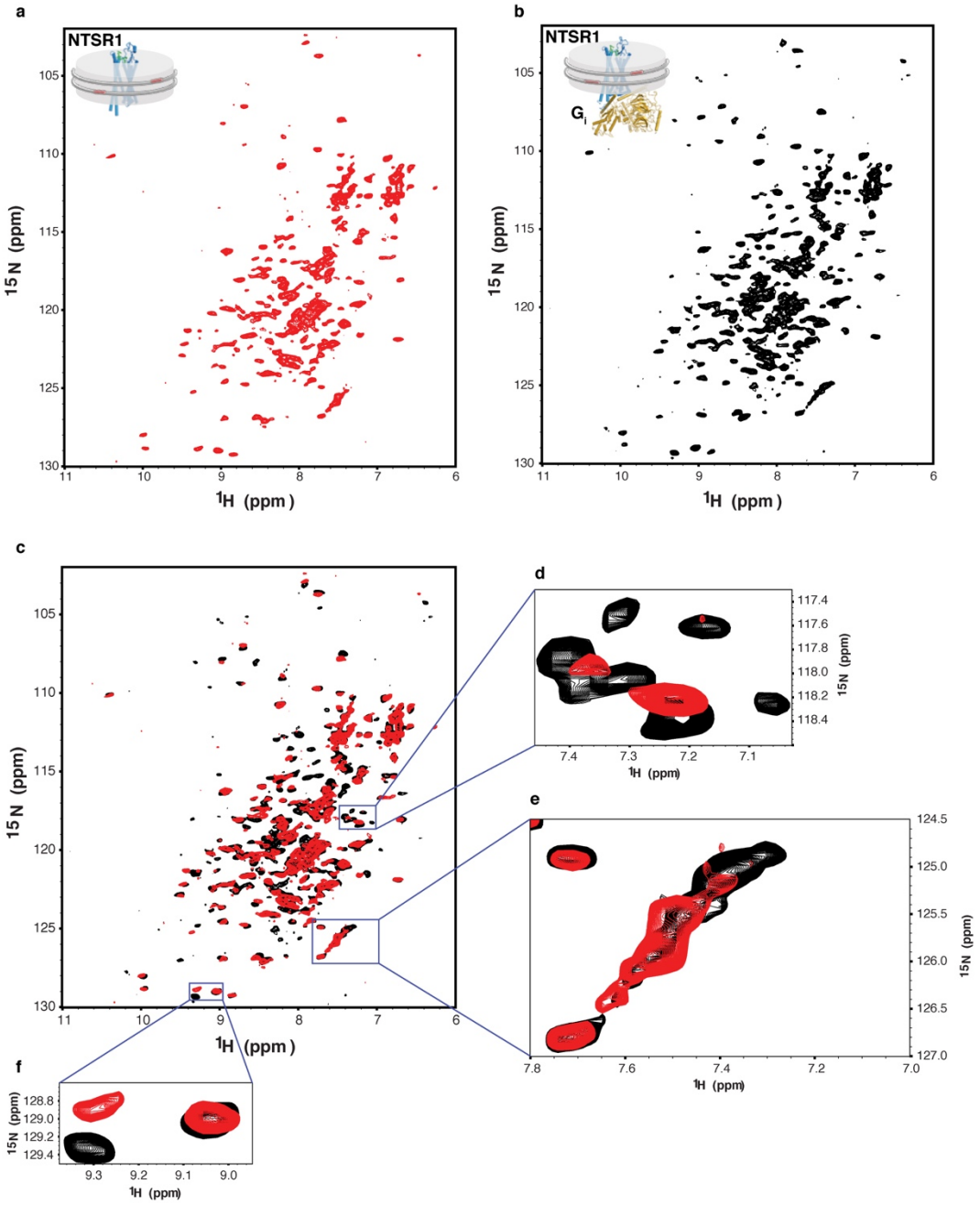

Supplementary Fig. 2 | Characterization of the interaction between NTS-NTSR1 and G_i in cNDs by two-dimensional ^{1}H, ^{15}N-TROSY HSQC NMR spectroscopy. **a-b**, NMR spectrum of ^{15}N-labeled NTS-NTSR1 in cNDs in the (**a**) absence and (**b**) presence of G_i. **c,** Overlay of (**a**) (red) onto (**b**) (black) showing structural and dynamical changes of NTS-NTSR1 upon binding to G_i in cNDs. **d**, A region showing conformational stabilization of NTSR1. More peaks are observed in

the presence of G_i, suggesting that NTSR1 is highly dynamic in the absence of G_i and resonances are averaged out among a wide range of conformers resulting in low signal-to-noise ratio and even disappeared peaks. Upon interaction with G_i, NTSR1 is stabilized into fewer conformers and becomes less dynamic, which leads to better signal-to-noise ratio and more resonances being observed. **e**, A region showing dynamically slow-exchange shift of NTSR1 upon interaction with G_i. **f**, A region showing chemical shift perturbation of NTSR1, suggesting conformational change of NTSR1 upon binding to G_i in cNDs.